SpezialForschungsBereich F 32

Karl–Franzens Universität Graz
Technische Universität Graz
Medizinische Universität Graz

Total Variation Regularization for Nonlinear Fluorescence Tomography With an Augmented Lagrangian Splitting Approach

Manuel Freiberger Christian Clason

Hermann Scharfetter

SFB-Report No. 2009–082 December 2009

A–8010 GRAZ, HEINRICHSTRASSE 36, AUSTRIA

Supported by the
Austrian Science Fund (FWF)

Der Wissenschaftsfonds.

SFB sponsors:

- **Austrian Science Fund** (FWF)
- **University of Graz**
- **Graz University of Technology**
- **Medical University of Graz**
- **Government of Styria**
- **City of Graz**

Total Variation Regularization for Nonlinear Fluorescence Tomography With an Augmented Lagrangian Splitting Approach

Manuel Freiberger *Student Member, IEEE*, Christian Clason, and Hermann Scharfetter

Abstract

Fluorescence tomography is a diffusion limited imaging modality which seeks to reconstruct the distribution of fluorescent dyes inside a sample from light measurements on the boundary. Using common inversion methods with L^2 penalties typically leads to smooth reconstructions which degrades the obtainable resolution. In this publication the use of total variation (TV) regularization for the inverse model is investigated. To solve the inverse problem efficiently, an augmented Lagrange method is utilized which allows separating the Gauß-Newton minimization from the TV minimization. Results on noisy simulation data provide evidence that the reconstructed inclusions are much better localized and that their half-width measure decreases by at least 25 % compared to the ordinary L^2 reconstructions.

I. Introduction

Fluorescence diffusion optical tomography (FDOT) is a promising imaging technique whose use in pre-clinical experiments is steadily increasing. The modality records the light emitted by fluorescent targets inside a biological sample on the sample's surface and seeks to reconstruct the three-dimensional fluorophore concentration. Various systems using intensity modulated light [1], [2] or time of flight measurements [3] have been reported over the years.

The technique is gaining interest as the optical properties of the fluorescent targets are influenced by its surrounding making FDOT sensitive to metabolic states and processes. Publications showed the

Manuscript received ??; revised ??. This work was supported by the project F3207-N18 granted by the Austrian Science Fund.

M. Freiberger and H. Scharfetter are with the Institute of Medical Engineering, Graz University of Technology, Kronesgasse 5/II, 8010 Graz, Austria. e-mail: {manuel.freiberger,hermann.scharfetter}@tugraz.at

C. Clason is with the Institute for Mathematics and Scientific Computing, University of Graz, Heinrichstr. 36/III, 8010 Graz, Austria. e-mail: christian.clason@uni-graz.at

dependence of the fluorescent dyes on the oxygen concentration [4], [5], the temperature [6] or the pH value [7], [8], for example.

In literature often linearized models for the light propagation are utilized such as the well-known Born approximation [9], [10] in order to reduce the numerical effort required for the solution of the forward and inverse problem. Frequently the inverse problem is solved with a linear regularization term based on the L^2 norm, for example [11].

FDOT is limited by the massive scattering of photons in most biological tissues leading to a resolution which is considerably worse than that of magnetic resonance imaging or x-ray tomography, for example. To mitigate for this lack of resolution, non-linear regularization methods such as total variation (TV) regularization can be used.

The main idea behind TV regularization is to penalize variations of the reconstructed parameter (the fluorophore concentration) and to favor larger regions with constant concentrations and sharp transitions between objects and the background, thus. One possible application might be the reconstruction of fluorescent dye in tumor tissue which is embodied in a non-fluorescent surrounding.

In section II-A the mathematical principle is introduced. In section II-B we give an efficient numerical implementation based on an augmented Lagrange method. Reconstruction results from simulated data using linear and non-linear regularization terms are presented in III.

II. Methods

A. Forward model

Light propagation of tissue is frequently modeled by the diffusion approximation which is a reduced form of Boltzmann's transport equation for highly scattering media. A derivation of the model and its limitations can be found in [12]. We utilize a coupled system of partial differential equations to describe the propagation of the excitation light (subscript ex) and the light emitted (subscript em) by the fluorophore [13].

$$-\nabla\cdot(\kappa_{ex}(x)\nabla\varphi_{ex}(x))+\left(\mu_{a,i,ex}(x)+c(x)\varepsilon_{ex}+\frac{i\omega}{v_{ex}}\right)\varphi_{ex}(x)=q(x),\qquad\text{in }\Omega \tag{1}$$

$$-\nabla\cdot(\kappa_{em}(x)\nabla\varphi_{em}(x))+\left(\mu_{a,i,em}(x)+c(x)\varepsilon_{em}+\frac{i\omega}{v_{em}}\right)\varphi_{em}(x)=\frac{Q}{1-i\omega\tau}c(x)\varepsilon_{ex}\varphi_{ex}(x),\qquad\text{in }\Omega. \tag{2}$$

In the equations above κ denotes the diffusion coefficient and $\mu_{a,i}$ the intrinsic absorption coefficient of the tissue at the respective wavelength. The quantity of interest is c which is the concentration of the fluorophore. ε is the molar extinction coefficient used to convert the concentration to an absorption

coefficient. The light intensity is modulated by the angular frequency ω. The excitation source term is denoted by q. τ is the lifetime of the fluorophore and Q its quantum efficiency. The equations are valid inside the domain. On the surface the Robin-type boundary conditions

$$\varphi_i(x) + 2R_i\kappa_i(x)\frac{\partial\varphi_i(x)}{\partial n} = 0, \qquad \text{on } \partial\Omega, \tag{3}$$

are used which have the same appearance for the excitation as for the emission wavelength. n is the outward-pointing unit-normal of the domain and R a reflection coefficient.

A measurement m is defined as the emitted photons leaving the domain at the detector site Γ_D:

$$m := -\int_{\Gamma_D} \kappa_i(x)\frac{\partial\varphi_i(x)}{\partial n}. \tag{4}$$

A typical setup can consist of s sources and d detectors distributed around the sample giving $s \times d$ measurements. The forward operator F relates a given fluorophore concentration c to the vector of measurements y:

$$F : c \to y, \qquad \text{where } c(x) \in \mathbb{R}^+ \text{and } y \in \mathbb{C}^{s\times d} \tag{5}$$

B. Inverse model

The inverse problem consists of finding a suitable fluorophore concentration $\tilde{c}$ from a set of measurements y^δ which are corrupted by noise. This can be achieved by minimizing the data error $\|F(c) - y^\delta\|^2$. As this constitutes an ill-posed problem [14], [12], a regularization term R must be added such that the problem reads

$$\tilde{c} = \min_c \|F(c) - y^\delta\|^2 + \alpha R(c). \tag{6}$$

As in this publication the forward operator depends non-linearly on c, we employ an iteratively regularized Gauss-Newton method [15], [16], [17], [18], i.e., for given c^k, solve

$$\min_{\delta c} \frac{1}{2}\|F(c^k) + F'(c^k)\delta c - y^\delta\|^2 + \alpha_k R(c^k + \delta c) \tag{7}$$

set $c^{k+1} = c^k + \delta c$, $\alpha_{k+1} < \alpha_k$ and iterate.

Typically the regularization term is an L^2 norm penalizing the difference between the reconstructed fluorophore concentration and some a priori guess c^p: $R(c) = \frac{1}{2}\|c - c^p\|^2$. The drawback of this method is that the reconstructed objects are diffuse and the image is smoothed. Therefore, in this paper a total variation (TV) regularization for FDOT is investigated. The total variation of a (sufficiently smooth) function u is defined as

$$TV(c) := \int |\nabla c| dx. \tag{8}$$

It is known that this penalty favors piecewise constant functions, and is much better suited for preserving jumps in the reconstruction. Since it is only a semi-norm, and we wish to incorporate a priori information in the form of c^p, we add a small L^2 penalty:

$$\alpha_k R(c) = \beta TV(c) + \frac{\alpha_k}{2}\|c - c^p\|^2. \tag{9}$$

Here, we do not wish to take β to zero, since we want to enforce the structural properties of TV minimizers for all iterates.

However, this regularization term is no longer differentiable, and so the minimizer can no longer be explicitly computed. On the other hand, while there exist efficient methods for TV minimization such as Chambolle's algorithm [19], [20], these become infeasible in the presence of operator terms like $F'(c^k)$. Therefore, we split the problem by introducing the new variable $\bar{c} = c^{k+1} = c^k + \delta c$ and replacing the TV term $TV(c^k + \delta c)$ with $TV(\bar{c})$. We then use an augmented Lagrangian approach [21], [22] to enforce the constraint $c^k + \delta c = \bar{c}$, which leads to the saddle point problem

$$\min_{\delta c, \bar{c}} \max_{\lambda} \frac{1}{2}\|F'(c^k)\delta c + F(c^k) - y^\delta\|^2 + \frac{\alpha_k}{2}\|c^k + \delta c - c^p\|^2 + \beta TV(\bar{c}^k) + \langle \lambda, c^k + \delta c - \bar{c}\rangle + \frac{\mu}{2}\|c^k + \delta c^k - \bar{c}^k\|^2, \tag{10}$$

where λ is the Lagrange multiplier associated with the equality constraint and the Lagrangian has been augmented by a penalization of the constraint with a fixed parameter $\mu > 0$. This additional penalization leads to improved the convergence of the method detailed below. The saddle point $(\delta c^*, \bar{c}^*, \lambda^*)$ can be found by alternately minimizing with respect to δc and $\bar{c}$ and updating the Lagrange multiplier using a gradient ascent step. This approach is known as the alternating direction minimization (ADM) method [23], [24], [25], and related splitting approaches have recently been applied successfully in the context of non-smooth image reconstruction problems [26], [27], [28]. The full procedure is given in Algorithm 1.

We next address the solution of the sub-problems. Minimizing (10) with respect to δc for given $\bar{c}$ and λ leads to the following standard linear least squares problem

$$\min_{\delta c} \frac{1}{2}\|F'(c^k)\delta c + F(c^k) - y^\delta\|^2 + \frac{\alpha_k}{2}\|c^k + \delta c - c^p\|^2 + \langle \lambda, \delta c\rangle + \frac{\mu}{2}\|c^k + \delta c - \bar{c}\|^2, \tag{11}$$

where we ignore the terms which are constant in δc. The minimizer is given by the solution of the normal equation,

$$[F'(c^k)^H F'(c^k) + (\alpha_k + \mu)I]\delta c = F'(c^k)(y^\delta - F(c^k)) - \alpha_k(c^k - c^p) - \mu(c^k - \bar{c}) - \lambda \tag{12}$$

Algorithm 1 ALM-ADM TV Gauß-Newton algorithm

Set $k = 0$, $\bar{c}^0 = c^p$, $\lambda^0 = 0$, choose α_0, q_α, β, μ

repeat ▷ Gauß-Newton loop

  Set $j = 0$

  repeat ▷ ADM loop

    Compute δc^{j+1} as minimizer of

$$\min_{\delta c} \frac{1}{2}\|F'(c^k)\delta c + F(c^k) - y^\delta\|^2 + \frac{\alpha_k}{2}\|c^k + \delta c - c^p\|^2 + \langle \lambda^j, \delta c\rangle + \frac{\mu}{2}\|c^k + \delta c - \bar{c}^j\|^2$$

  by solving (12)

    Compute $\bar{c}^{j+1}$ as minimizer of

$$\min_{\bar{c}} \beta TV(\bar{c}) - \langle \lambda^j, \bar{c}\rangle + \frac{\mu}{2}\|c^k + \delta c^{j+1} - \bar{c}\|^2$$

  using Algorithm 2

    Set $\lambda^{j+1} = \lambda^j + \mu(c^k + \delta c^{j+1} - \bar{c}^{j+1})$, update $j \leftarrow j + 1$

  until $|c^k + \delta c^j - \bar{c}^{j-1}|^2 < tol$

  Set $c^{k+1} = \bar{c}^j = c^k + \delta c^j$

  Update $\alpha_{k+1} = q_\alpha \alpha_k$, $k \leftarrow k + 1$

until $\|F'(c^k)\| < \varepsilon$

which can be efficiently computed using the CG method. The minimization with respect to $\bar{c}$ for given $c^{k+1} = c^k + \delta c$ and λ is equivalent to TV denoising:

$$\min_{\bar{c}} \beta TV(\bar{c}) - \langle \lambda, \bar{c}\rangle + \frac{\mu}{2}\|c^{k+1} - \bar{c}\|^2, \tag{13}$$

again ignoring terms independent of $\bar{c}$. For the solution of this sub-problem, we employ Nesterov's optimal rate gradient descent method [29] to the dual problem of (13), which has been shown to have significantly better performance than Chambolle's algorithm [30], [31]. Using standard tools from convex analysis [32], the dual problem is found to be

$$\min_{\|p\|_\infty \leq \beta} \frac{1}{2\mu}\| - \operatorname{div} p + \lambda\|^2 + \langle -\operatorname{div} p, c^{k+1}\rangle, \tag{14}$$

where p denotes the dual variable. We therefore have to minimize a smooth functional with Lipschitz continuous gradient over a convex feasible set $K = \{p : \|p\|_\infty \leq \beta\}$. Nesterov's method is a projected gradient descent method, in which the convergence is accelerated by using in each iteration information

Algorithm 2 Nesterov's method for TV minimization

INPUT $c^{k+1}, \lambda, \beta, \mu, L, N$

Set $x^0 = 0$, $q^0 = 0$

for $k = 1, \ldots, N$ **do**

$\eta^k = \nabla \left(\frac{1}{\mu}(-\operatorname{div} x^k + \lambda) + c^{k+1} \right)$

$y^k = x^{k-1} - \eta^k / L$

$y^k = \frac{\beta y^k}{\max(\beta, |y^k|)}$

$q^k = q^{k-1} + \frac{k+1}{2}\eta^k$

$z^k = q^k / L$

$z^k = \frac{\beta z^k}{\max(\beta, |z^k|)}$

$x^k = \frac{2}{k+3} z^k + \frac{k+1}{k+3} y^k$

end for

OUTPUT $\bar{c} = \frac{1}{\mu}(-\operatorname{div} y^N + \lambda) + c^{k+1}$.

from previous gradients as well as the gradient at the current iterate. The optimal convergence rate for first order schemes is achieved by a suitable convex combination of these gradients.

In the case of problem (14), the gradient of the functional to be minimized is given by

$$\nabla \left(\frac{1}{\mu}(-\operatorname{div} p + \lambda) + c^{k+1} \right) \tag{15}$$

with Lipschitz constant $L = \frac{12}{\mu}$, and the projection of a vector v onto the set K can be easily calculated as

$$P_K(v) = \frac{\beta v}{\max(\beta, |v|)}, \tag{16}$$

where the $\max$ is taken component-wise. Applying Nesterov's method to problem (14) yields Algorithm 2. After the dual minimizer p^* is computed, we can recover the desired TV minimizer $\bar{c} = \frac{1}{\mu}(-\operatorname{div} p^* + \lambda) + c^{k+1}$.

III. Numerical experiment

Simulation data was gathered using a finite element discretization of a cylindrical mesh with a radius of $15\,\mathrm{mm}$ and a height of $60\,\mathrm{mm}$. We positioned 24 source optodes and an equal number of detectors on three rings around the cylinder with a spacing in z-direction of $10\,\mathrm{mm}$ (see Fig. 1). The material values

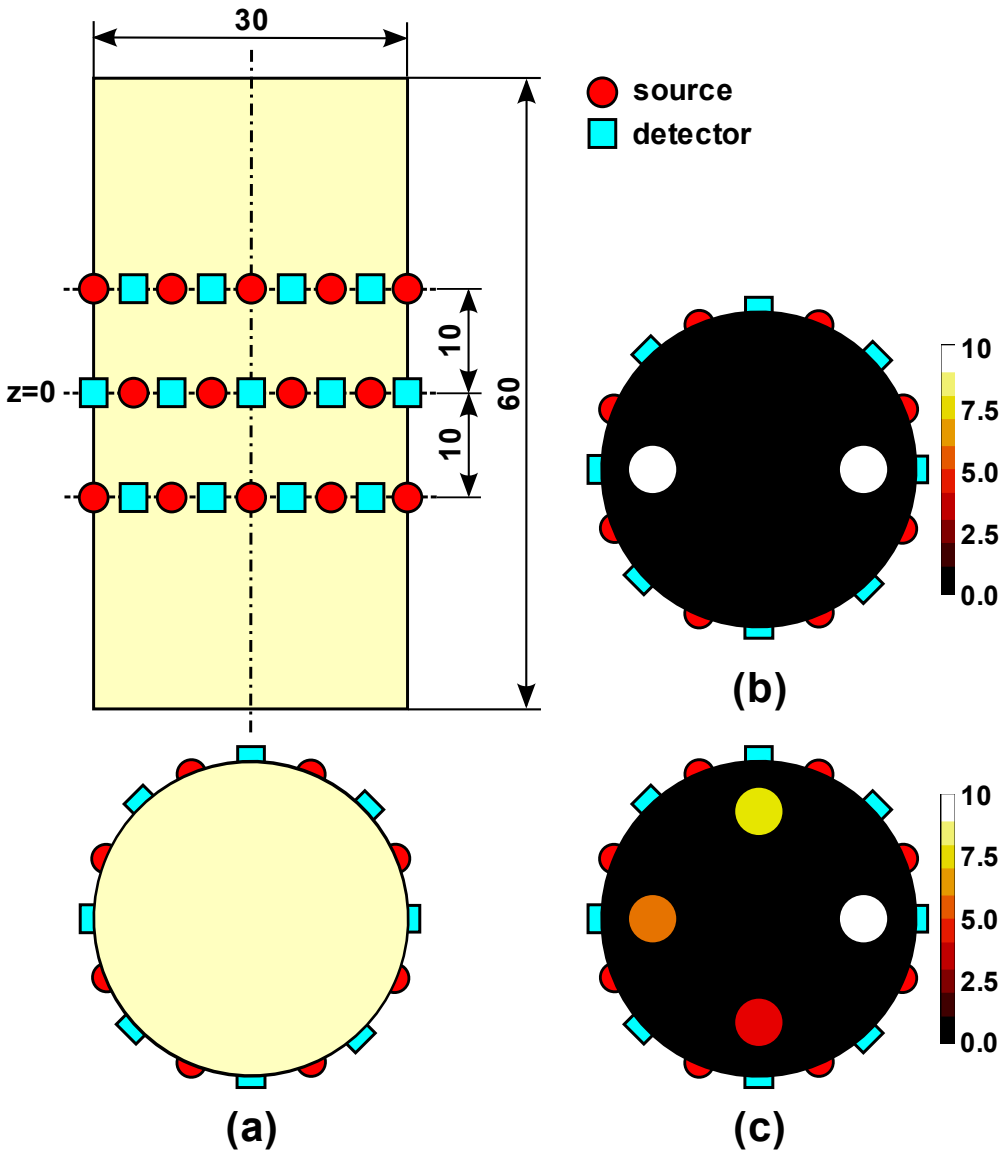

Fig. 1. Geometry and source and detector placement used for the simulations (a) and two simulation phantoms (b,c) with spherical inclusions (concentrations in μM)

used for the simulations were compiled from various literature sources [33], [34], [13], and are given in Table I.

To avoid committing an inverse crime, two different finite element grids were used for the computation of the measurement data and the reconstructions. Additionally, Gaussian noise was added to the simulated data before reconstruction. In order to solve the inverse problem, it was assumed that the tissue properties were known beforehand such that the only unknown is the fluorophore distribution c in (1). These

TABLE I

LIST OF OPTICAL TISSUE PARAMETERS USED FOR THE COMPUTATION OF MEASUREMENT DATA [33], [34], [13]

Wavelength	μ_s'	$\mu_{a,i}$	ε	R
	mm^{-1}	mm^{-1}	$\mathrm{mm}^{-1}\,\mathrm{M}^{-1}$	
excitation	0.275	0.036	8.4×10^3	2.51
emission	0.235	0.029	2.5×10^3	2.51

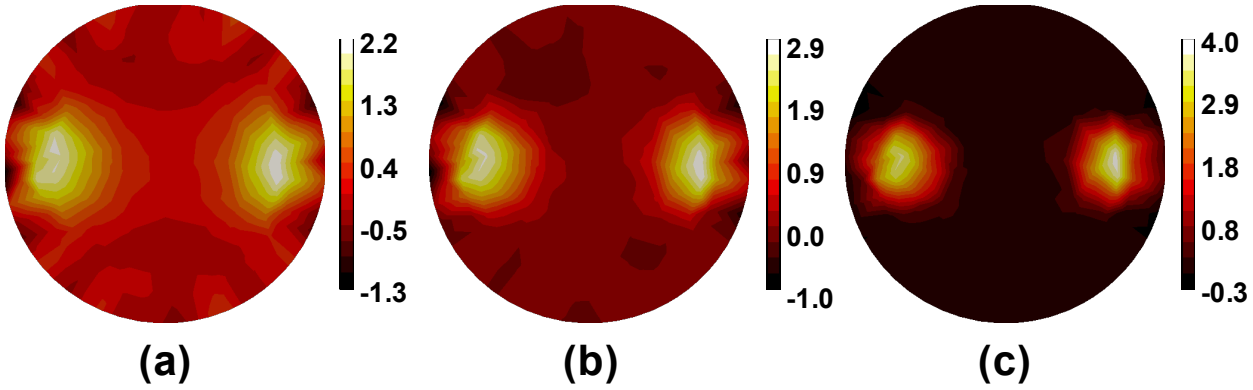

Fig. 2. Reconstruction results of the phantom shown in Fig. 1(b) with L^2 regularization (a) and two TV reconstructions using a lower penalty (b) and a higher one (c).

quantities could be estimated through, e.g., additional a priori measurements.

A. *Influence of TV regularization*

The first test case consists of two spherical fluorescent targets with a concentration of $10\,\mu\mathrm{M}$ and a diameter of $5\,\mathrm{mm}$ inside the cylinder at a depth of $5\,\mathrm{mm}$, as depicted in Fig. 1(b).

In this test, $3\,\%$ of Gaussian noise was added to the measurement data. The L^2-regularized reconstruction shown in Fig. 2(a) correspond to the regularization parameters $\alpha_0 = 1 \times 10^{-2}$ and $q_\alpha = 0.2$. For the TV reconstructions, the parameters were set to $\alpha_0 = 1 \times 10^{-2}$, $q_\alpha = 0.2$, $\mu = 1 \times 10^{-7}$. The regularization parameter β controlling the influence of the TV penalty on the minimization functional was set to 2×10^{-11} for Fig. 2(b) and to 1×10^{-10} for 2(c). The Gauß-Newton iteration was stopped according to Morozov's discrepancy principle [35], [16], *i.e.* when the data residual fell below the noise level. The ADM loop is stopped after 10 iterations or when the difference of $c^k + \delta c$ to $\bar{c}$ is less then $1\,\%$. The reconstructed concentrations have been scaled to the maximum in each image.

It is clearly visible that the L^2 reconstruction exhibits ringing artifacts near the fluorescent inclusions which degrade image quality significantly. This makes it rather hard to estimate the border between an object and the background. Also, the reconstructed inclusions show a significant spread compared to the true locations which is inherent in most diffusion-limited imaging modalities. It can be noticed that the radial localization is slightly better than the angular one.

The addition of a small TV penalty (Fig. 2(b)) is already sufficient to enforce a nearly homogeneous background which makes it easier to discriminate between the perturbations and the background. The inclusions have almost the same size and shape as the ones in the L^2 regularized images. When the TV penalty is increased further, the perturbations are confined to a smaller volume which improves the localization of the fluorescent spheres (Fig. 2(c)).

B. Influence of data noise

The second test case consists of four spherical fluorescent targets inside the cylindrical phantom. Each inclusion has got a diameter of $5\,\mathrm{mm}$. Concentration of $10\,\mu$M, $8\,\mu$M, $6\,\mu$M and $4\,\mu$M have been assigned to the inclusions in counter-clockwise orientation starting from the right-most sphere (see Fig. 1(c)).

The reconstructions are performed with the same parameters as in III-A. This time the TV regularization parameter is fixed to $\beta = 1 \times 10^{-10}$. Fig. 3 shows reconstruction results using the L^2 and the TV regularization for noise levels of $0\,\%$, $5\,\%$ and $10\,\%$. The reconstructed concentration is mapped to $\mathbb{R}^+$ for the evaluation of the images. The white border around the inclusions depicts the full-width at half-maximum (FWHM). For the noise-free case the reconstruction was stopped after 15 iterations as Morozov's discrepancy principle does not apply in this case.

Looking at the reconstructions in Fig. 3(a,c,e) it can be seen that the radial resolution of the L^2 regularized images is better compared to the angular one. This is not the case applying TV regularization where the resolution is much more isotropic as is visible in Fig. 3(b,d,f). If no noise is present, the L^2 reconstructions give slightly better results in terms of reconstructed concentration and size of the reconstructed objects (compare Fig. 3(a) and (b)). This is due to the fact that the TV reconstruction method converges slower because of the additional non-linearity. The only advantage of the total variation method is in this case the suppression of the artifacts near the cylinder boundary which can be noticed when closely looking at Fig. 3(a). However, is is obvious the L^2 reconstructions degrade quickly with increasing noise level. The total variation reconstructions are much more stable with respect to noise both in terms of reconstructed parameter value and object size.

In Table II the maximum fluorophore concentration and the maximum FWHM diameter of every

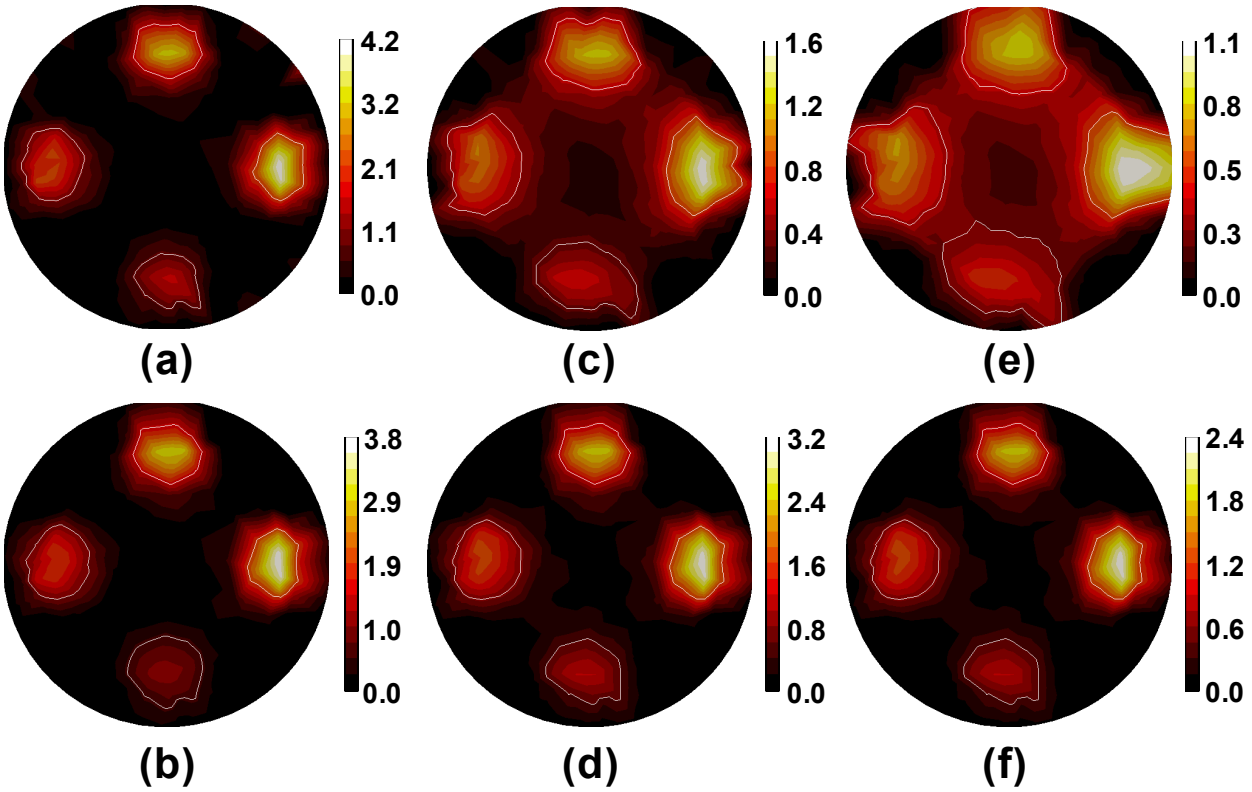

Fig. 3. L^2 regularized (upper row) and total variation reconstructions (lower row) for different noise levels of 0 % (left), 5 % (middle) and 10 % (right) data noise. The white border marks the FWHM.

reconstructed fluorescent inclusion is listed. Both regularization strategies exhibit concentration values which are smaller compared to the original concentration, which is due to the fact that the fluorescent spheres appear diffused. For the noise-free case the L^2 method reconstructs more correct concentration values. However, in case of noise the total variation regularization outperforms L^2 quite clearly.

Comparing the largest FWHM diameter, it is obvious that the TV reconstructions are superior to the L^2 regularized images if noise is present. The difference is in the order of 20 % to 25 % for a noise level of 5 % and increases up to at 35 % for 10 % noise. This shows that the total variation regularization can improve the localization of the fluorescent inclusions and is much more stable at higher noise levels.

Finally, Table III shows the number of Gauß-Newton iterations needed for each test case until the L^2 or the total variation regularized images exhibit a data residual which is below the noise level. The TV method needs more iterations due to the additional non-linearity of the regularization term.

TABLE II

MAXIMUM CONCENTRATION AND FWHM OF THE RECONSTRUCTED FLUORESCENT INCLUSIONS. E (EAST), S (SOUTH), W (WEST) AND N (NORTH) DENOTE THE LOCATION OF THE INCLUSION.

Noise	Sphere location	Concentration (μM)			FWHM (mm)		
		original	L^2	TV	L^2	TV	difference
0 %	E	10.0	4.23	3.84	6.2	6.3	-2 %
	N	8.0	3.33	3.05	6.3	6.4	-2 %
	W	6.0	2.25	1.92	6.8	6.9	-1 %
	S	4.0	1.71	1.08	6.8	7.1	-4 %
5 %	E	10.0	1.61	3.17	9.1	6.7	26 %
	N	8.0	1.47	2.50	8.8	6.5	26 %
	W	6.0	1.29	1.71	9.4	7.4	21 %
	S	4.0	0.86	1.21	10.0	7.5	25 %
10 %	E	10.0	1.06	2.41	9.7	7.5	23 %
	N	8.0	0.85	1.92	10.6	6.9	35 %
	W	6.0	0.75	1.49	11.0	8.0	27 %
	S	4.0	0.53	1.07	12.9	8.4	35 %

TABLE III

NUMBER OF GAUSS-NEWTON ITERATIONS UNTIL CONVERGENCE.

Test case	L^2	TV
2 inclusions, 3 % noise	8	10 ($\beta = 2 \times 10^{-11}$)
		16 ($\beta = 1 \times 10^{-10}$)
4 inclusions, 5 % noise	7	11
4 inclusions, 10 % noise	6	9

IV. DISCUSSION

Fluorescence optical tomography suffers from reduced resolution in comparison to, e.g., magnetic resonance imaging or X-ray computed tomography. Using an L^2 regularization term, the resultant images appear often too smooth (see Fig. 2(a), for example). An intuitive but non-mathematical explanation is that in every reconstruction step only linear combinations of the singular vectors of the sensitivity matrix F' are added to the reconstructed image. However, the singular vectors of F' are smooth over the image

due to the diffusive nature of light transport in highly scattering media. One possibility to overcome this problem is to employ non-linear methods.

As was shown in this paper the TV model is well suited to reconstructing smaller inclusions in an otherwise non-fluorescent surrounding. The suppression of ringing artifacts and the resultant uniformity of the background aids the visual detection of fluorescent inclusions. Furthermore, the total variation regularization concentrates the fluorescent inclusions much better, improving the localization of the perturbations. L^2 regularization is only advantageous in the unrealistic case of noise-free data due to its faster convergence.

The reconstruction method presented above requires the choice of several parameters compared to standard L^2-Tikhonov regularization, which might be seen as a disadvantage. However, the only regularization parameter (in the sense that its choice influences the reconstruction result) is the TV penalty β. The additional L^2 penalty α is necessary to ensure numerical stability of the normal equation (11), and can be made as close to zero as desired during the Gauß-Newton iteration. Similarly, the ADM method converges for every choice of the augmented Lagrangian penalty $\mu > 0$, while the precise value of μ has effect only on the speed of convergence of the ADM.

The parameters given in section III-A were chosen heuristically to obtain sufficiently fast convergence, but proved to be stable and usable for a series of similar images i.e. small inclusions inside a homogeneous object. While outside the scope of the current paper, it is possible to adapt model function approaches for the automatic choice of these parameters based on path-following [36], [37] (for μ and α) or balancing principles [38], [39], [27], [40] (for β).

The splitting approach presented in this paper has the advantage that the Gauß-Newton step and the TV term can be solved independently by applying optimized algorithms for each of the sub-problems. A further speed-up of the method is possible by parallelization of the TV code. See [41] and the references cited therein for a discussion on this topic.

REFERENCES

[1] J. S. Reynolds, T. L. Troy, and E. M. Sevick-Muraca, "Multipixel techniques for frequency-domain photon migration imaging," *Biotechnol. Prog.*, vol. 13, pp. 669–690, 1997.

[2] A. B. Milstein, S. Oh, K. J. Webb, C. A. Bouman, Q. Zhang, D. A. Boas, and R. P. Millane, "Fluorescence optical diffusion tomography," *Applied Optics*, vol. 42, pp. 3081–3094, 2003.

[3] D. S. Elson, I. Munro, J. Requejo-Isidro, J. McGinty, C. Dunsby, N. Galletly, G. W. Stamp, M. A. A. Neil, M. J. Lever, P. A. Kellett, A. Dymoke-Bradshaw, J. Hares, and P. M. W. French, "Real-time time-domain fluorescence lifetime imaging including single-shot acquisition with a segmented optical image intensifier," *New Journal of Physics*, vol. 6, p. 180, 2004. [Online]. Available: http://stacks.iop.org/1367-2630/6/180

[4] I. S. Longmuir and J. A. Knopp, "Measurement of tissue oxygen with a fluorescent probe," *J Appl Physiol*, vol. 41, no. 4, pp. 598–602, 1976. [Online]. Available: http://jap.physiology.org/cgi/content/abstract/41/4/598

[5] E. Shives, Y. Xu, and H. Jiang, "Fluorescence lifetime tomography of turbid media based on an oxygen-sensitive dye," *Opt. Express*, vol. 10, pp. 1557–1562, 2002.

[6] Y. Y. Chen and A. W. Wood, "Application of a temperature-dependent fluorescent dye (rhodamine b) to the measurement of radiofrequency radiation-induced temperature changes in biological samples," *Bioelectromagnetics*, vol. 30, pp. 583–590, 2009.

[7] S. Mordon, V. Maunoury, J. M. Devoisselle, Y. Abbas, and D. Coustaud, "Characterization of tumorous and normal tissue using a pH-sensitive fluorescence indicator (5,6-carboxyfluorescein) in vivo." *J Photochem Photobiol B*, vol. 13, no. 3-4, pp. 307–314, May 1992.

[8] I. Gannot, I. Ron, F. Hekmat, V. Chernomordik, and A. Gandjbakhche, "Functional optical detection based on pH dependent fluorescence lifetime." *Lasers Surg Med*, vol. 35, no. 5, pp. 342–348, 2004. [Online]. Available: http://dx.doi.org/10.1002/lsm.20101

[9] M. A. O'Leary, D. A. Boas, X. D. Li, B. Chance, and Y. G. Yodh, "Fluorescence lifetime imaging in turbid media," *Opt. Lett.*, vol. 21, pp. 158–160, 1996.

[10] V. Ntziachristos and R. Weissleder, "Experimental three-dimensional fluorescence reconstruction of diffuse media by use of a normalized born approximation," *Optics Letters*, vol. 26, pp. 893–895, 2001.

[11] A. Joshi, W. Bangerth, and W. M. Sevick-Muraca, "Adaptive finite element based tomography for fluorescence optical imaging in tissue," *Opt. Express*, vol. 12, pp. 5402–5417, 2004.

[12] S. R. Arridge, "Optical tomography in medical imaging," *Inverse Problems*, vol. 15, pp. R41–R93, 1999.

[13] A. Joshi, "Adaptive finite element methods for fluorescence enhanced optical tomography," Ph.D. dissertation, Texas A&M University, 2005.

[14] H. Egger, M. Freiberger, and M. Schlottbom, "Analysis of foward and inverse models in fluorescence optical tomography," SFB Report, Tech. Rep. 2009-075, 2009. [Online]. Available: http://math.uni-graz.at/mobis/publications/SFB-Report-2009-075.pdf

[15] A. B. Bakushinsky and M. Y. Kokurin, *Iterative methods for approximate solution of inverse problems*, ser. Mathematics and Its Applications (New York). Dordrecht: Springer, 2004, vol. 577.

[16] H. W. Engl, M. Hanke, and A. Neubauer, *Regularization of Inverse Problems*. Dordrecht: Kluwer, 1996.

[17] B. Blaschke, A. Neubauer, and O. Scherzer, "On convergence rates for the iteratively regularized Gauss-Newton method," *IMA J. Numer. Anal.*, vol. 17, no. 3, pp. 421–436, 1997.

[18] T. Hohage, "Logarithmic convergence rates of the iteratively regularized Gauss-Newton method for an inverse potential and an inverse scattering problem," *Inverse Problems*, vol. 13, no. 5, pp. 1279–1299, 1997.

[19] A. Chambolle, "An algorithm for total variation minimization and applications," *J. Math. Imaging Vision*, vol. 20, no. 1-2, pp. 89–97, 2004, special issue on mathematics and image analysis.

[20] ——, "Total variation minimization and a class of binary MRF models," in *EMMCVPR*, 2005, pp. 136–152.

[21] M. R. Hestenes, "Multiplier and gradient methods," *J. Optimization Theory Appl.*, vol. 4, pp. 303–320, 1969.

[22] M. J. D. Powell, "A method for nonlinear constraints in minimization problems," in *Optimization (Sympos., Univ. Keele, Keele, 1968)*. London: Academic Press, 1969, pp. 283–298.

[23] R. Glowinski and A. Marrocco, "Sur l'approximation, par éléments finis d'ordre 1, et la résolution, par pénalisation-dualité, d'une classe de problèmes de Dirichlet non linéaires," *C. R. Acad. Sci. Paris Sér. A*, vol. 278, pp. 1649–1652, 1974.

[24] D. Gabay and B. Mercier, "A dual algorithm for the solution of nonlinear variational problems via finite element approximation." *Comput. Math. Appl.*, vol. 2, pp. 17–40, 1976.

[25] R. Glowinski, *Numerical Methods for Nonlinear Variational Problems*, ser. Scientific Computation. Berlin: Springer-Verlag, 2008, reprint of the 1984 original.

[26] T. Goldstein and S. Osher, "The split Bregman method for L1-regularized problems," *SIAM Journal on Imaging Sciences*, vol. 2, no. 2, pp. 323–343, 2009. [Online]. Available: http://link.aip.org/link/?SII/2/323/1

[27] C. Clason, B. Jin, and K. Kunisch, "A duality-based splitting method for ℓ^1-TV image restoration with automatic regularization parameter choice," SFB Report, Tech. Rep. 2009-041, 2009. [Online]. Available: http://math.uni-graz.at/mobis/publications/SFB-Report-2009-041.pdf

[28] M. Tao and J. Yang, "Alternating direction algorithms for total variation deconvolution in image reconstruction," TR0918, Department of Mathmatics, Nanjing University, November, 2009. [Online]. Available: http://www.optimization-online.org/DB_HTML/2009/11/2463.html

[29] Y. Nesterov, "Smooth minimization of non-smooth functions," *Math. Program.*, vol. 103, no. 1, Ser. A, pp. 127–152, 2005.

[30] P. Weiss, L. Blanc-Féraud, and G. Aubert, "Efficient schemes for total variation minimization under constraints in image processing," *SIAM J. Sci. Comput.*, vol. 31, no. 3, pp. 2047–2080, 2009. [Online]. Available: http://dx.doi.org/10.1137/070696143

[31] J.-F. Aujol, "Some first-order algorithms for total variation based image restoration," *J. Math. Imaging Vision*, vol. 34, no. 3, pp. 307–327, 2009. [Online]. Available: http://dx.doi.org/10.1007/s10851-009-0149-y

[32] I. Ekeland and R. Témam, *Convex Analysis and Variational Problems*. Philadelphia, PA, USA: Society for Industrial and Applied Mathematics, 1999.

[33] G. Alexandrakis, F. R. Rannou, and A. F. Chatziioannou, "Tomographic bioluminescence imaging by use of a combined optical-pet (opet) system: a computer simulation feasibility study," *Physics in Medicine and Biology*, vol. 50, pp. 4225–4241, 2005.

[34] M. Keijzer, W. M. Star, and P. R. M. Storchi, "Optical diffusion in layered media," *Applied Optics*, vol. 27, pp. 1820–1824, 1988.

[35] V. A. Morozov, "On the solution of functional equations by the method of regularization," *Soviet Math. Dokl.*, vol. 7, pp. 414–417, 1966.

[36] M. Hintermüller and K. Kunisch, "Path-following methods for a class of constrained minimization problems in function space," *SIAM Journal on Optimization*, vol. 17, no. 1, pp. 159–187, 2006. [Online]. Available: http://link.aip.org/link/?SJE/17/159/1

[37] G. Stadler, "Path-following and augmented Lagrangian methods for contact problems in linear elasticity," *J. Comput. Appl. Math.*, vol. 203, no. 2, pp. 533–547, 2007. [Online]. Available: http://dx.doi.org/10.1016/j.cam.2006.04.017

[38] K. Ito and K. Kunisch, "On the choice of the regularization parameter in nonlinear inverse problems," *SIAM J. Optim.*, vol. 2, no. 3, pp. 376–404, 1992.

[39] K. Kunisch and J. Zou, "Iterative choices of regularization parameters in linear inverse problems," *Inverse Problems*, vol. 14, pp. 1247–1264, 1998.

[40] C. Clason, B. Jin, and K. Kunisch, "A semismooth newton method for l1 data fitting with automatic choice of regularization parameters and noise calibration," SFB Report, Tech. Rep. 2009-015, 2009. [Online]. Available: http://math.uni-graz.at/mobis/publications/SFB-Report-2009-015.pdf

[41] T. Pock, M. Unger, D. Cremers, and H. Bischof, "Fast and exact solution of total variation models on the GPU," in

Computer Vision and Pattern Recognition Workshops, 2008. CVPRW '08. IEEE Computer Society Conference on, 2008, pp. 1–8. [Online]. Available: http://dx.doi.org/10.1109/CVPRW.2008.4563099